Electrotaxis of oral squamous cell carcinoma cells in a multiple-electric-field chip with uniform flow field

Hsieh-Fu Tsai,[1,2,3] Shih-Wei Peng,[1,2,3] Chun-Ying Wu,[2,4] Hui-Fang Chang,[2] and Ji-Yen Cheng[1,2,3,4,a)]

[1]*Institute of Biophotonics, National Yang-Ming University, Taipei 11221, Taiwan*
[2]*Research Center for Applied Sciences, Academia Sinica, Taipei 11529, Taiwan*
[3]*Biophotonics and Molecular Imaging Research Center (BMIRC), National Yang-Ming University, Taipei 11221, Taiwan*
[4]*Department of Mechanical and Mechatronic Engineering, National Taiwan Ocean University, Keelung 20224, Taiwan*

(Received 15 June 2012; accepted 20 August 2012; published online 5 September 2012)

We report a new design of microfluidic chip (**M**ultiple electric **F**ield with **U**niform **F**low chip, MFUF chip) to create multiple electric field strengths (EFSs) while providing a uniform flow field simultaneously. MFUF chip was fabricated from poly-methyl methacrylates (PMMA) substrates by using CO_2 laser micromachining. A microfluidic network with interconnecting segments was utilized to de-couple the flow field and the electric field (EF). Using our special design, different EFSs were obtained in channel segments that had an identical cross-section and therefore a uniform flow field. Four electric fields with EFS ratio of 7.9:2.8:1:0 were obtained with flow velocity variation of only 7.8% CV (coefficient of variation). Possible biological effect of shear force can therefore be avoided. Cell behavior under three EFSs and the control condition, where there is no EF, was observed in a single experiment. We validated MFUF chip performance using lung adenocarcinoma cell lines and then used the chip to study the electrotaxis of HSC-3, an oral squamous cell carcinoma cell line. The MFUF chip has high throughput capability for studying the EF-induced cell behavior under various EFSs, including the control condition (EFS = 0). © *2012 American Institute of Physics*. [http://dx.doi.org/10.1063/1.4749826]

INTRODUCTION

Electrotaxis, or galvanotaxis, is the directional migration of adherent cells toward either cathode or anode under a direct current electric field (dcEF). From early research, electrotaxis has been known to play a profound role in embryonic development, neurogenesis, and wound healing.[1,2] Many different cell types and organisms show electrotactic response to dcEF, including neural stem cell,[3] induced pluripotent stem cells,[4] mesenchymal stem cells,[5,6] fibroblasts,[7–9] keratinocytes,[10,11] neurons,[2] and *C. elegans*.[12,13] The physiological dcEF with strength of tens to hundreds of mV per mm ($mV \cdot mm^{-1}$) originates from the difference in transepithelial potential (TEP), which is supposedly formed by the differential distribution of ion channels on polarized epithelial cells.[1,14] In recent years, many groups have reported that cancer cells also show electrotactic behavior. The electrotactic directionalities of different cancer cell types also correlate with the TEPs of the corresponding tissues.[15–19]

The mechanisms of cell electrotaxis have been investigated over the past few decades but have been found to be complex and differ between cell types.[1] Several models of dcEF detection and signal transduction have been proposed. The most accepted model is asymmetrical distribution of cell membrane receptors driven by the EF-induced *in situ* electrophoresis[20,21] or

a)Author to whom correspondence should be addressed. Electronic mail: jycheng@gate.sinica.edu.tw. Tel.: +886-2-27898000#34. Fax: +886-2-27826680.

electro-osmosis.[22] Asymmetrical distribution of receptors such as epidermal growth factor receptors (EGFR),[17] vascular endothelial growth factor receptor (VEGFR),[23,24] hepatocyte growth factor receptors(HGFR),[25] or Na/K ATPase[26] results in enhanced signaling on a single side of the cells. Involvement of voltage-gated sodium channel[16] or voltage-gated calcium channel[27] activated by dcEF has also been reported. In past studies, many signaling pathways involved in electrotaxis of numerous cell types have also been investigated. The intracellular biochemical signaling pathways include small GTPases,[28] MAPK/ERK,[17,25] and phosphoinositide-3 kinase pathways(PI3K).[29] In cancer cells, activations of these signaling pathways would contribute to cell proliferation, anti-apoptosis, and angiogenesis. These studies suggest a possible link between electrotaxis and cancer metastasis. Therefore we are interested in the electrotactic response of cancer cells.[18,30–32]

Conventional methods to investigate electrotaxis using a dish-based device[33–35] or a transwell assay[36] have been reported in detail. However, conventional methods have drawbacks including low experimental throughput, lack of miniaturization, complex assembly, risk of contamination, and medium evaporation.[37]

In electro-microfluidics where ionic solutions can be considered as Ohmic resistors, the resistance of each microfluidic segment is determined by the resistivity of the residing fluid, the length of the segment, and the cross-sectional area of the segment. To create multiple uniform electric fields in several microfluidic segments, manipulation of cross-sectional area is the most direct way. In our previous work, we have utilized a PMMA microfluidic device, MFC, to overcome the disadvantages of the conventional methods by miniaturizing the experimental setup and increasing the experimental throughput.[18] A micro-channel has been designed to have three consecutive segments with a width ratio of 1:3:5 and an EFS ratio inversely proportional to the segment width. Cell electrotaxis under different EFSs has been studied in one experiment using MFC. The overall experiment time is thus shortened compared to those using the conventional methods.

However, the varied widths in the consecutive segments in MFC result in a flow velocity ratio that is proportional to the EFS. In consequence, the segment with the highest EFS also has the highest flow velocity and vice versa. Furthermore, the influence on cells by the variation in the flow velocity and the accompanying shear force difference has been studied extensively in the field of mechanobiology. Overlapping signaling pathways such as Rho small GTPase in both EF-induced cell orientation and shear stress-induced cell alignment have been reported for endothelial cells.[23,38] These reports suggest the requirement of a uniform flow velocity during the investigation of electrotaxis.

An additional drawback arising from different flow velocities is the uneven cell distribution in the MFC electrotaxis chip.[18] High flow velocity in the narrow segment results in low cell density and therefore limits the amount of cells that can be observed in a single experiment. Also, in MFC, separate experiments are required for the control condition (EFS = 0 mV/mm).

In this study, we report a new design, MFUF chip, to create multiple EFSs based on an interconnecting network of microfluidic segments. A main channel is divided into four main segments by three narrower segments. The four main segments have identical cross-section and therefore a comparable internal flow velocity in the four segments could be expected. In this way, the EFS and flow field distribution in the network are expected to be de-coupled. One of the four segments is an EF-null segment that can be used for the control experiment. Thus, the need to perform a separate control experiment is averted.

MATERIALS AND METHODS

MFUF chip microfluidic network design

Fig. 1(a) shows the microfluidic network in MFUF chip to obtain multiple EFSs. The region between inlet 1 and the outlet is the 4 mm-wide main channel. The main channel is divided into four main segments (I, II, III, and IV in Fig. 1(a)) by vertical segments with width of 1 mm, 1 mm, and 2 mm, respectively, from the left to the right. The central regions in the four main segments are used for cell observation in this study. A 1 mm-wide channel connects

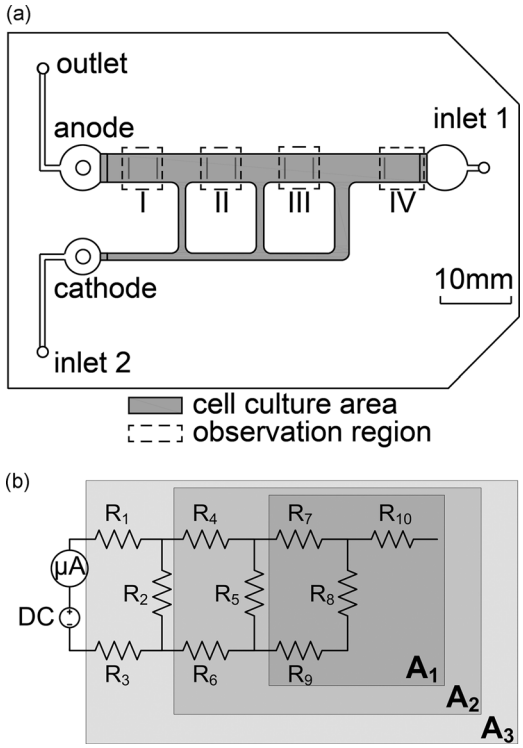

FIG. 1. (a) The top view of MFUF showing the geometry of the microfluidic chamber and the cell culture area. The observation regions are selected in the middle of each segment where homogeneous electric fields are obtained. (b) The equivalent circuit of MFUF.

the vertical segments to the cathode. During EF stimulation, culture medium was introduced into and pumped through the network via inlet 1 to the outlet. Please note that the port combinations for introducing the medium and the EF are different. All segments have the same length (10 mm) except segment IV, which is 11 mm. The length of segment IV was tentatively increased to keep the observation region away from the EF-stimulated region.

For a simplified electrical analysis of the microfluidic network, all segments are considered as resistors and denoted as R_i, $i = 1$ to 10. The equivalent circuit of Fig. 1(a) is then constructed and shown in Fig. 1(b). The equivalent circuit can be treated as three C-section circuits, A_1, A_2, and A_3. Additional segments in the main channel can be added by inserting additional C-sections between the connections of anode-R_1 and cathode-R_3. With the increased number of C-sections, more EFSs can be obtained in the main channel. Because the segment R_{10} is not included in the electric circuit between the cathode and the anode, there should be no current flowing through R_{10}. Therefore this segment can be used for the control experiment, in which the EFS should be zero.

By analyzing this parallel circuit according to Kirchhoff's voltage law and Ohm's law, the voltage ratio of the four segments, I, II, III, and IV, as denoted by V_{R1}, V_{R4}, V_{R7}, and V_{R10} is calculated to be 7.93:2.75:1:0. See section I in the supplementary material[39] for detailed equations and analysis.

Fabrication of MFUF chip

The configuration of MFUF chip for electrotaxis is shown in Fig. 2. To begin MFUF chip fabrication, channel patterns on three PMMA layers were plotted in AutoCAD (AutoDESK, USA). These patterns are for connecting the cell culturing region to the reagent ports. The patterns were then cut on a piece of 1 mm-thick PMMA substrate by using a CO_2 laser scriber (ILS-II, LTT Group, Taiwan). The three PMMA layers were thermally bonded to form the top

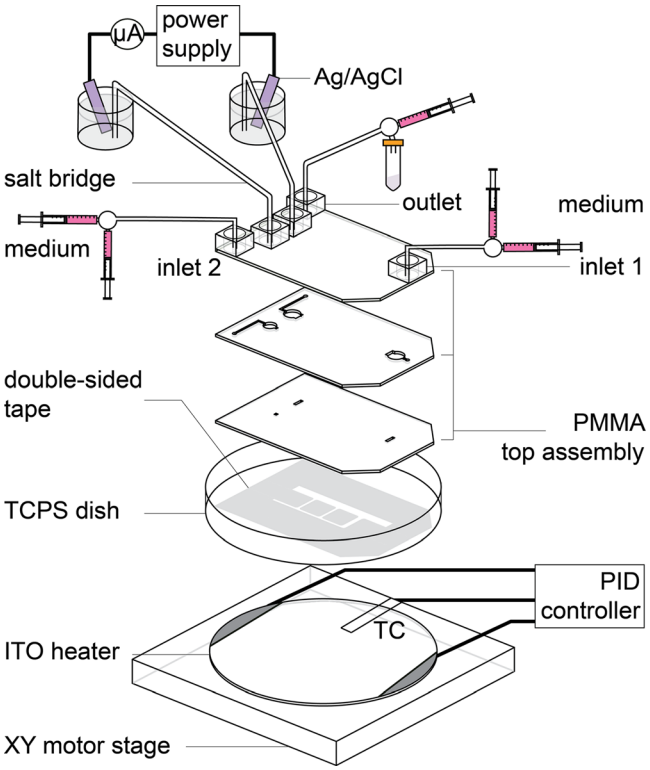

FIG. 2. The setup scheme of electrotaxis experiment. The PMMA top assembly is adhered on a TCPS dish and fixed on an ITO heater for cell culturing. Medium was pumped through the microfluidic channel by a syringe pump. A direct current is applied through the salt bridges to form multiple electric fields in the chip. TC: Thermocouple.

assembly. Adapters for fitting connection were glued on the top assembly afterward. The detail of the PMMA laser machining technique has been reported in our previous works.[32,40,41]

The microfluidic network shown in Fig. 1(a) was patterned by CO_2 laser ablation on a piece of 70 μm-thick polyester double-sided tape (PET 8018, 3 M, USA) adhered on a Teflon film (ASF-110, Chukoh Ltd., Japan). The biocompatibility of the double-sided tape has been confirmed in our previous study.[41] The Teflon film acts as a releaser to hold isolated parts of the double-sided tape during the patterning process. After disinfection by UV light exposure for 30 min, the top assembly was affixed to the patterned double-sided tape and then adhered onto a tissue culture poly-styrene (TCPS) dish (430167, Corning, USA) to complete the MFUF chip. The MFUF chip was then put in a vacuum chamber for 30 min to reach firm affixation. We found that the vacuuming step was crucial for long-term bubble-free cell culturing.

Cell culture and maintenance

Two lung adenocarcinoma cell lines, CL1-0 and CL1-5, were gifts from Dr. Pan-Chyr Yang, National Taiwan University Hospital.[42] Both cell lines were derived from a parental clinical isolate CL1. CL1-0 cells show low invasiveness while CL1-5 cells present high invasiveness in both *in vivo* and *in vitro* experiments.[43]

A moderately differentiated oral squamous cell carcinoma cell line with lymph node metastasis, designated as HSC-3, originally from Japan Health Science Research Resources Bank (HSRRB, Tokyo, Japan) was a gift from Dr. Yuh-Shan Jou, Institute of Biomedical Sciences, Academia Sinica.[44,45]

CL1 Cells were cultured in Dulbecco's modified Eagle Medium (DMEM, GIBCO, Invitrogen, USA), and HSC-3 cells were cultured in DMEM-F12 medium, both media supplemented with 10% fetal bovine serum (FBS, HyClone, Thermo Scientific, USA), in TCPS flasks (3290, Corning, USA) under 37 °C moist atmosphere with 5% CO_2. The cells were passaged every 3

to 4 days. The cells used in this work were within 10 to 20 passages. The cultured cells are routinely tested for mycoplasma by a commercial PCR kit (e-Myco plus, iNtRON Biotech, Korea). All the cells used in this study are free of mycoplasma contamination.

Numerical simulation of electric field and flow field

The electric field and flow field in MFUF chip were numerically simulated using commercial software CFD-GEOM, CFD-ACE+, and CFD-VIEW (ESI Group, France). The *DC conduction* module was used in the electric field simulation and the electrical conductivity of the medium was set as $1.38\,S{\cdot}m^{-1}$ for DMEM.[46] For *fluidic field volume condition*, a parameter used by CFD-ACE+, the model based on liquid water with viscosity of $0.00078\,kg{\cdot}m^{-1}{\cdot}s^{-1}$ was used in the simulation.[47]

Electric field strength measurement

Electric field measurement in the regions for cell observation was carried out as follows. Opening holes near the cell observation region were designed on the MFUF chip and drilled by the CO_2 laser scriber. Home-made silver-silver chloride (Ag/AgCl) electrodes were inserted in adjacent holes. The voltage drops (ΔV) between two adjacent holes were measured by a multifunction data acquisition card (NI-USB-6216, National Instruments, USA) with a home-written LABVIEW program at the sampling rate of $400\,kS{\cdot}s^{-1}$. The EFS was calculated by dividing the measured ΔV by the distance between two adjacent holes. See section III.1 in the supplementary material[39] for detailed description of measurement process.

Electrotaxis experiment

As shown in Fig. 2, the syringes for introducing cells and medium were connected to the inlets of MFUF through 3-way stopcocks (NIPRO, Japan), Teflon tubing and fittings (IDEX Corp., USA). The MFUF chip was sequentially flushed from inlet 1 and inlet 2 to the outlet with CO_2 air and $1\times$ Dulbecco's modified phosphate buffered saline (PBS, AMRESCO, USA). The chip was then filled with a complete medium of DMEM supplemented with 10% FBS and was ready for cell seeding.

Before cell seeding, MFUF chip was stacked on top of a transparent heater made of indium tin oxide glass (ITO glass, part No. 300739, Merck). The stacked chip was clamped on an X-Y motorized stage (Tanlian Inc., Taiwan) mounted on an inverted phase contrast microscope (CKX41, Olympus, Japan). A Z-axis motor was used to adjust the objective position to correct focuses at the four cell observation regions, I, II, III, and IV. For introducing electric field to the chip, salt bridges composed of silicone tubes filled with 1.5% agar (Sigma-Aldrich, USA) in $1\times$ PBS were connected to the chip via the anode port and the cathode port. The distal ends of the salt bridges were immersed in vials containing PBS and the electrodes. See Fig. S2 in the supplementary material[39] for the photo picture of the setup.

The ITO heater, a K-type thermocouple (TPK-02 A, Tecpel Inc., Taiwan), and a PID controller (TTM-J40-R-AB, Toho Electronics, Japan) were utilized to maintain the temperature of MFUF chip at $37 \pm 0.3\,^{\circ}C$ to allow suitable cell growth. The transparent ITO heater allows simultaneous temperature control and real-time cell observation. The detailed information of the ITO planar heater and its application in microfluidic chip have been reported in detail in our previous work.[41]

To prepare cells for electrotaxis, cultured cells were washed by $1\times$ PBS and then trypsinized (0.25% Trypsin-EDTA, Invitrogen, USA) from TCPS flask. The trypsin was removed by centrifugation and cells were re-suspended in CO_2-equilibrated DMEM supplemented with 10% FBS to a concentration of $0.5–2\times10^7$ cells/mL. 0.3 mL cell suspension was injected into MFUF chip via the outlet, with inlet 1 and inlet 2 opened, in order to avoid bubbles. Monolayer dispersed cells were allowed to adhere on the TCPS surface at $37\,^{\circ}C$ for three hours. After the cells adhered, inlet 2 was sealed, and CO_2-equilibrated DMEM with 10% FBS was pumped through the cell culture region via inlet 1 and flowed to the outlet at $20\,\mu l/h$ using a syringe

pump (NE-1000, New Era Pump Systems, Inc.). The cells in the chip were cultured for 16 h prior to the following procedures for the application of dcEF.

For serum-free medium condition, the medium in the chamber was substituted by serum-free DMEM (abbreviated as SF-DMEM below) before the dcEF application. Briefly, SF-DMEM was infused from inlet 2, with inlet 1 closed and the outlet opened at 10 μl/min for 10 min and then inlet 2 was sealed. Later, SF-DMEM was infused from inlet 1, with the outlet opened, at 10 μl/min for 10 min. Then, SF-DMEM was continuously infused from inlet 1 to the outlet at the infusion rate of 20 μl/h during the EF stimulation. The flow direction is from EF-null region (segment IV) to EF-stimulated regions (consecutively segments III, II, and I) and is expected to avoid the effect of signaling molecules secreted by up-stream EF-stimulated cells to non-stimulated cells during the electrotaxis experiment. For serum-containing condition, all infusion and washing procedures were the same as those for serum-free condition except that serum-containing medium was used.

To introduce EF stimulation, a direct current ($115.9 \pm 0.5\,\mu$A for EFS = 300 mV/mm in segment I) was applied through the Ag/AgCl plate electrodes in the PBS buffer by a DC power supply (GPS-3030DQ, GW Instek, Taiwan). The use of Ag/AgCl instead of platinum electrode is crucial for preventing *p*H changes during the electrotaxis experiment. The required current was calculated by Ohm's Law, $I = \sigma EA$, where the current, I, equals to the product of conductivity σ of the medium, electric field E in the corresponding segment, and cross-sectional area A of the segment.

Cell imaging and time-lapse microphotography

A digital SLR camera (Canon 60D, Japan) was mounted on the CKX41 microscope for time-lapse imaging. An input/output (I/O) board (Arduino Uno) controlled relay was used to turn on the electrical power of the microscope light source during only image taking, avoiding prolonged light exposure to the cells and excessive heating of the microscope optics. Images of cells in the regions with homogenous EF were taken for analysis. A home-written MATLAB GUI program was used for coordinating the motion of the motorized stage, the Arduino I/O board, and the time-lapse image taking by the camera.

Image analysis and data processing

Time-lapse images from the phase contrast microscopy were analyzed by the Fiji ImageJ distribution[48] with the built-in measurement tool and the *region-of-interest* (ROI) manger. All adherent cells in the images were manually selected as ROIs. The position of a cell is defined by its centroids. The long axis of a cell is defined as the major axis of the best-fit ellipse of the cell outline. The orientation of a cell is defined as the angle between the cell's long axis and the EF vector direction, as illustrated in the inset of Fig. 6. The cells that divided during the experiment were excluded for analysis.

For each experiment condition, totally over 80 cells from three independent experiments were analyzed. Euclidean distance, migration speed, directedness, and orientation were calculated for each cell.

Non-parametric statistical inference was performed on all data. The confidence level to reject a null hypothesis was represented by the P-value in corresponding figures. A P-value less than 0.05 represents a statistical significance. All bar charts were presented by sample means with error bars indicating the 95% confidence interval. In all figures, the asterisk (*) denotes $p < 0.05$ and the double asterisks (**) denote $p < 0.001$. See section III.2 in the supplementary material[39] for the detailed definition of the properties and the description of statistical inference.

RESULTS AND DISCUSSIONS

Simulation and measurement of the electric field and the flow field

Fig. 3(a) shows the numerical simulation result of EFS distribution in MFUF. The four segments in the main channel showed obvious stepwise changes in the EFS. Fig. 3(b) shows the simulated and the measured EFS in the four segments. Homogeneous EF distribution was

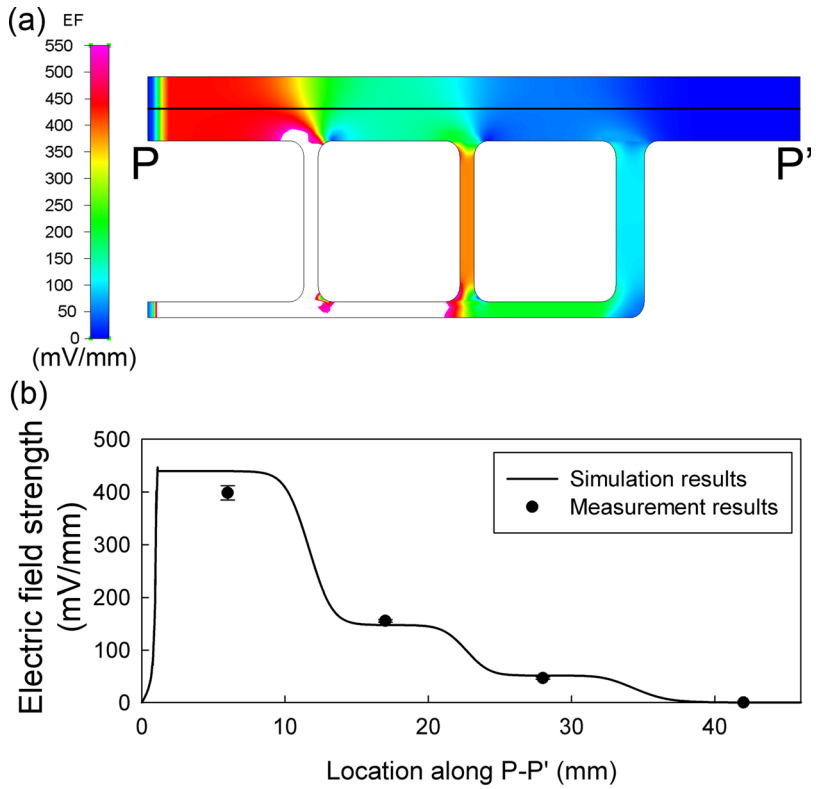

FIG. 3. (a) The simulated electric field distribution in MFUF at 170 μA. (b) Comparison between the simulated and the measured EF along the cross-section P-P′ in (a).

observed in the center region of each of the four segments. The cell images during the electrotaxis experiments were taken in the homogeneous regions.

From the calculation using the equivalent circuit, the EFS ratio of the four segments was 7.9:2.8:1:0. For comparison, the simulation gave a ratio of 8.6:2.9:1:0. The measurement by Ag/AgCl electrodes gave a ratio of 8.5:3.4:1:0. The difference between the EFS measurements and the numerical simulation was less than 10%. The EF homogeneity within each main segment was also analyzed. The coefficient of variations of the simulated EFS within the cell observation regions of segment I, II, and III are 1.8%, 4.2%, and 4.9%, respectively. The numerical simulation shows homogeneous EF distribution in the observation regions of MFUF chip. In other words, behaviors of different cells in each homogeneous region can be grouped together to represent the cell behavior in each region. See Fig. S3 in supplementary material[39] for the 3D plot of the EFS distribution with EFS presented in height.

Our measurement also showed that a small EF existed along the vertical direction in the observation region. However, the vertical EFS was only a few mV/mm, which is smaller than 2% of the horizontal EFS. Therefore, the effect of the vertical EF was neglected.

In our previous report, multiple EFSs were obtained in the micro-channel but accompanied by non-uniform flow field in the cell culture region.[18] The flow velocity distribution in MFC, as shown in Fig. 4(a), increases in proportion to the increase of the EFS. Compared to MFC, the flow field in MFUF chip is very homogeneous, as shown in Fig. 4(b). By simulation, the flow velocity in the four segments of MFUF chip has a coefficient of variations of 7.8%. This result indicates that the microfluidic network successfully de-couples the electric field distribution from that of flow field. At a high flow rate of 20 μl/h (corresponding to flow velocity of 20 μm/s) in this work. The calculated shear rate is 0.0039 Pa (0.039 dyn·cm^{-2}).[49] The shear stress variation throughout the four segments is only 3.0×10^{-4} Pa.

For comparison, the physiologically relevant shear rates have been reported to be 0.2 to 1 Pa for leukocyte transendothelial migration[50] and 0.3 Pa for endothelial cell remodeling.[51] The

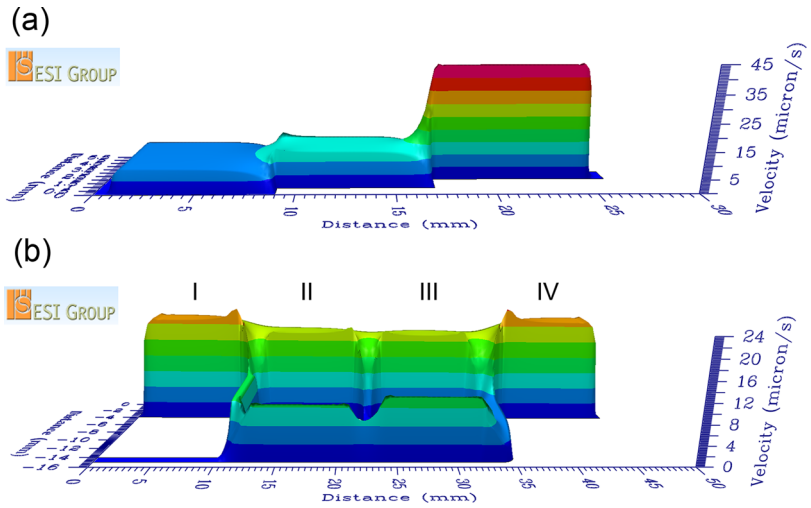

FIG. 4. The 3D plot of simulated flow field in (a) MFC and (b) MFUF. The height in the plots is in μm/s.

shear rate in MFUF chip is two orders of magnitude smaller than the physiologically relevant values. The relatively homogeneous flow velocity throughout the main channel in MFUF chip is expected to obviate the effect of different shear rates when investigating electrotaxis in high throughput scheme.

It should be mentioned that in such a microchamber, in which the thickness (70 μm) is significantly smaller than the width (4 mm), the flow field has flat flow front as in a Hele-Shaw flow cell[52,53] but is not parabolic, which is commonly observed for pressure-driven flow. The characterizations of a Hele-Shaw flow cell for cell culture have been described in our previous works.[18,41,54] Although the flow front is indeed parabolic along Z-axis, the adherent cells at different locations at the bottom of the microfluidic chamber should be subjected to the same shear rate.

Cell culture in bubble-free microfluidic environment

Because there are narrow segments (1 mm) in the MFUF chip design, formation of bubbles could easily affect the flow field and the electric field distribution. Large bubbles could even cause breakage in the circuitry and in turn disrupt the EF distribution. We found that by eliminating bubble forming using the vacuum pretreatment, we can confidently obtain a microfluidic chamber with homogeneous EF distribution for long-term (longer than one week) study. This is another improvement over the previous MFC study. See section IV.1 in the supplementary material[39] for the detailed discussion.

Validation of MFUF chip performance by lung adenocarcinoma cells

The performance of the MFUF chip for electrotaxis study was first validated by studying the behavior of CL1 lung adenocarcinoma cells under dcEF, which has been reported before. The quantitative results of directedness, speed, and orientation change of CL1-0 and CL1-5 cells after two hours of dcEF stimulation correlate well with our previous results.[18] In addition, there is no statistically significant difference in the directedness of CL1 cells between the EF null region (segment IV) and the control (no electric field application). This result demonstrated that, by using MFUF chip, data of the control group are acquired in a single experiment together with the EF-stimulated electrotaxis data. This characteristic further demonstrates the advantage of MFUF chip over the previous design. The detailed quantitative results and discussion can be seen in sections IV.2 and IV.3 in the supplementary material.[39]

In summary, the directed cell migration and the re-orientation of CL1-5 cells in MFUF chip confirmed the compatibility of this device for electrotaxis studies.

The electrotaxis of HSC-3 oral squamous cell carcinoma cells

We used MFUF chip to study the electrotaxis of HSC-3 cells in both serum-containing and serum-free media. The Euclidean migration distances of HSC-3 cells in the two conditions under different EFSs for two hours can be seen as polar plots in Fig. S4 in the supplementary material.[39] The quantitative analysis of HSC-3 electrotaxis directedness is shown in Fig. 5(a). HSC-3 showed correlated increase in directedness toward cathode with increasing EFSs compared to that in the EF null region. In serum-containing medium, the directedness of HSC-3 in the null region was -0.12 ± 0.14 (95% confidence interval) while under 104 mV/mm and 300 mV/mm, the directedness were 0.31 ± 0.14 and 0.48 ± 0.11, respectively. In contrast, the directedness of HSC-3 in serum-free medium under 300 mV/mm for two hours was 0.06 ± 0.12 and is not statistically significant compared to the result in the null region (-0.03 ± 0.14). The detailed quantitative result is listed in table.S1 in the supplementary material.[39]

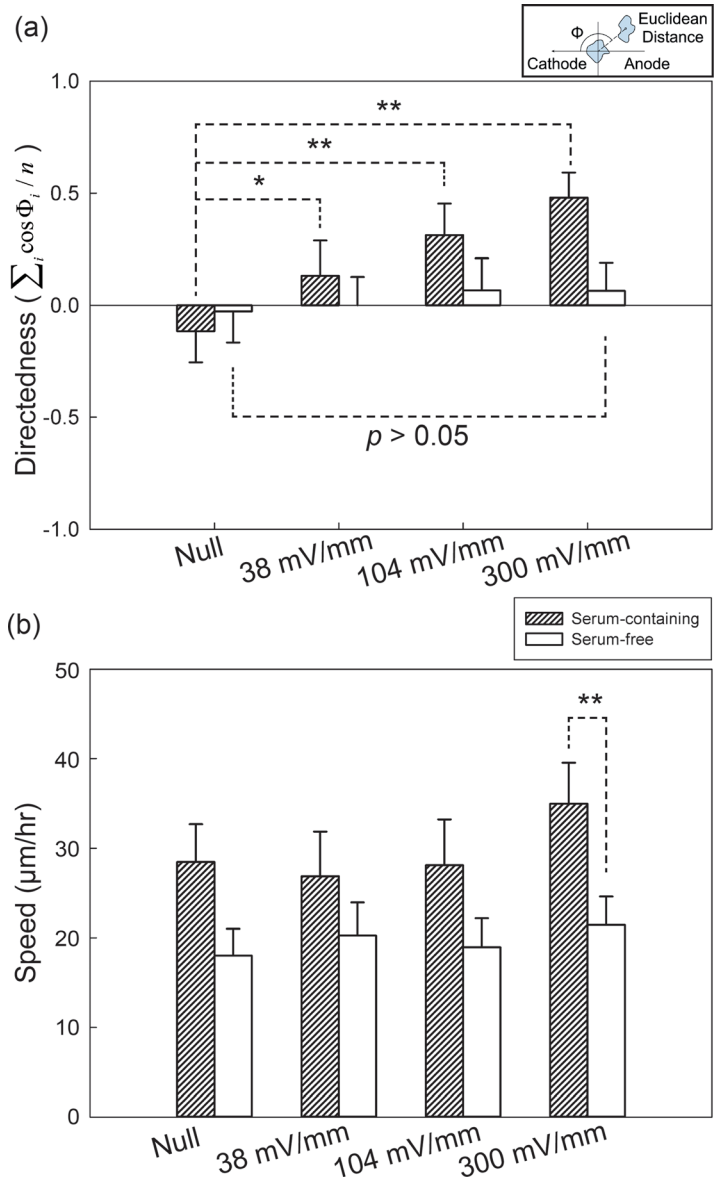

FIG. 5. (a) Directedness and (b) migration speed of HSC-3 cells under different conditions. The EF stimulation time was two hours. The inset in (a) shows the definition of directedness.

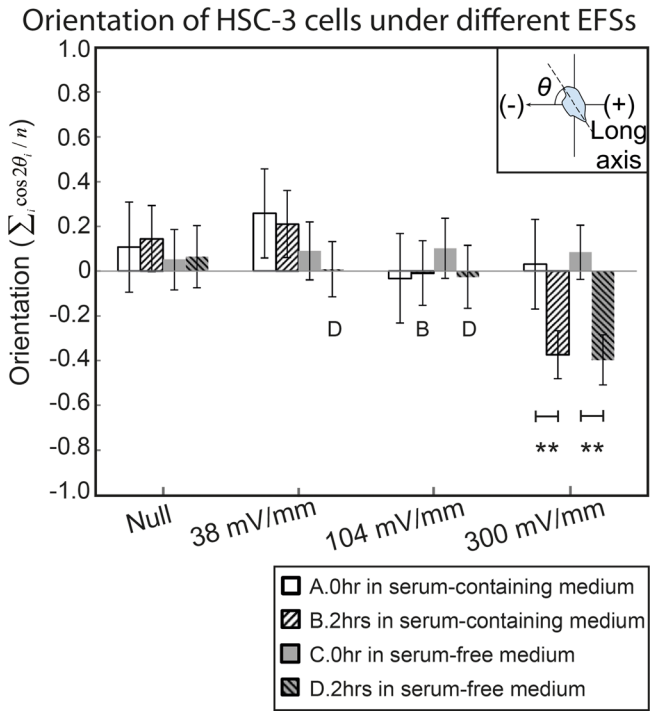

FIG. 6. The orientation of HSC-3 cells under different conditions before and after two hours EF stimulation. The inset shows the definition of orientation.

The average speed of HSC-3 electrotaxis under different EFSs were analyzed and shown in Fig. 5(b). HSC-3 cell migration speed in serum-containing medium was higher compared to that in serum-free medium ($p < 0.001$ by rank sum test). However, HSC-3 cell migration speed appears to be independent of EFSs compared to CL1-5 cells. In summary, our results showed that HSC-3 cell electrotaxis is serum dependent and HSC-3 cells migrated towards cathode.

In recent years, electrotaxis of many cancer cells have been reported. These include prostate cancer cells,[16] breast cancer cells,[17] and lung adenocarcinoma cells.[18,19,30] Cancer cells having higher metastatic potential also showed stronger electrotactic response. In this study, it is found that, although HSC-3 migrate faster than CL1-5 (28 μm/h vs. 5 μm/h under EFS = 0 mV/mm), the directedness of HSC-3 is not as significant as that of CL1-5 (+0.48 vs. −0.76 under EFS = 300 mV/mm). This result indicates that the cancer cells' motility alone is not necessarily correlated to the electro-response of the cells. Further investigation into cancer cell electrotaxis would help elucidating the role of physiological EF in cancer biology.

The orientation of HSC-3 cells under dcEF

The orientation changes of HSC-3 cells before and after two hours of dcEF stimulation were also analyzed. Aside from electrotaxis, cells may show perpendicular[55] or parallel[56] re-orientation of long axis after EF stimulation, named electro-alignment as below. The results of cell orientation under the different conditions are shown in Fig. 6, and the inset shows the definition of orientation. The orientation of cells was calculated by the average cosine 2θ, where θ is the angle between cell's long axis with EF vector. With or without serum, HSC-3 showed perpendicular alignment only under 300 mV/mm dcEF. Although the electrotaxis of HSC-3 is serum dependent, the electro-alignment of HSC-3 shows serum independency. This result suggests that the electrotaxis and the electro-alignment of HSC-3 cells may involve different cellular signaling pathways. Similar observations that suggest the involvement of the separate pathways has been reported before on CL1-5 lung adenocarcinoma cells and mice adipose-derived stromal cells.[5,18] The role of cancer cell electro-alignment in cancer morphogenesis and cancer development as well as intracellular signaling cascades involved in the behavior are largely unknown and require further research.

It should be emphasized that, in this study, the results with and without EF-stimulation were obtained in a same chip. The chip-to-chip variation could be further reduced compared to previous studies.

Further improvement

In our study, we found that MFUF chip greatly reduced the electrotaxis experiment time. However, the analysis of cell morphology, including cell migration and orientation, becomes the most time-consuming bottleneck procedure. In order to further improve the throughput of electrotaxis studies, automatic cell morphology analysis and cell tracking software need to be adapted. Phase contrast microscopy is an ideal method for cell motility study, but the artifacts such as shade off and halo make automatic cell segmentation difficult. To solve this problem, several software have been developed based on image segmentation methods such as active contour algorithm,[57,58] weak watershed transform assembly,[59] image registration,[60] or level-set method.[61] Implementation of automated cell segmentation and tracking software for time-lapse image analysis in future would further improve the throughput of electrotaxis experiment.

Currently, there has been no report on high-throughput screening device for studying the effect of chemicals on electrotaxis behavior. Therefore, such studies need to be carried out for each compound one-by-one. It is believed that such high-throughput screening device is worth of development.

CONCLUSION

In this study, we report a new microfluidic biochip, MFUF chip, to create multiple electric fields for the study of cell electrotaxis under a microscope. The **M**ultiple electric **F**ield with **U**niform **F**low chip, MFUF chip, has four major segments with EFS ratio of 7.9:3.8:1:0. In the four segments, comparable medium flow velocities were obtained. Electrotaxis of cells were observed under the three different EFSs and the control condition was obtained in the EF null region in the same experiment. In this way, the MFUF chip design improves the throughput of electrotaxis experiment. In MFUF chip experiments, we used the standard TCPS dish as the substrate. It is expected that various types of adherent cells can be easily studied using this system. Also, through the vacuum pretreatment, we achieved long-term bubble-free cell culture in the MFUF chip. This property is beneficial for long-term electrotaxis studies and avoids the harmful effect of interfacial phenomena on experimental cells

We validated the performance of MFUF chip using CL1-0 and CL1-5 lung adenocarcinoma cell lines. The electrotaxis of CL1 cells in MFUF chip was similar to that obtained in MFC, the predecessor of MFUF chip. The electrotaxis of HSC-3 was also studied by using MFUF chip. We showed that HSC-3 electrotaxis is serum dependent but electro-alignment is not. In addition, HSC-3 cells show weaker electrotaxis response although the motility is higher than CL1-5 cells.

The molecular mechanisms of how cancer cells sense the electric field and respond to it require further studies. Understanding of the role of physiological electric field in cancer biology could aid in cancer diagnosis or even cancer therapeutics. With several advantages of the new device, MFUF chip could help to expedite electrotaxis studies.

ACKNOWLEDGMENTS

This work is financially supported by the National Science Council, Taiwan (Contract No. 100-2113 -M-001-014-MY3) and the Research Program on Nanoscience and Nanotechnology, Academia Sinica, Taiwan. The authors also thank Dr. Ching-Wen Huang, Dr. Yung-Shin Sun, and Mr. Jia-Hau Chang for their valuable discussion on the development of the cell culture chip. We also thank Professor Jeff Yi-Fu Chen for his assistance in acquiring HSC-3 cell lines.

[1]C. D. McCaig, B. Song, and A. M. Rajnicek, J. Cell. Sci. **122**, 4267–4276 (2009).
[2]L. Yao, A. Pandit, S. Yao, and C. D. McCaig, Tissue Eng. Part B Rev. **17**(3), 143–153 (2011).
[3]L. Li, Y. H. El-Hayek, B. Liu, Y. Chen, E. Gomez, X. Wu, K. Ning, N. Chang, L. Zhang, Z. Wang, X. Hu, and Q. Wan, Stem Cells **26**(8), 2193–2200 (2008).

[4]J. Zhang, M. Calafiore, Q. Zeng, X. Zhang, Y. Huang, R. A. Li, W. Deng, and M. Zhao, Stem Cell Rev. **7**(4), 987–996 (2011).
[5]K. E. Hammerick, M. T. Longaker, and F. B. Prinz, Biochem. Biophys. Res. Commun. **397**(1), 12–17 (2010).
[6]S. Sun, I. Titushkin, and M. Cho, Bioelectrochemistry **69**(2), 133–141 (2006).
[7]A. Guo, B. Song, B. Reid, Y. Gu, J. V. Forrester, C. A. Jahoda, and M. Zhao, J. Invest. Dermatol. **130**(9), 2320–2327 (2010).
[8]E. Finkelstein, W. Chang, P. H. Chao, D. Gruber, A. Minden, C. T. Hung, and J. C. Bulinski, J. Cell. Sci. **117**(8), 1533–1545 (2004).
[9]J. Jennings, D. Chen, and D. Feldman, Bioelectromagnetics **29**(5), 394–405 (2008).
[10]K. Y. Nishimura, R. R. Isseroff, and R. Nuccitelli, J. Cell. Sci. **109**(1), 199–207 (1996).
[11]K. S. Fang, B. Farboud, R. Nuccitelli, and R. R. Isseroff, J. Invest. Dermatol. **111**(5), 751–756 (1998).
[12]P. Rezai, A. Siddiqui, P. R. Selvaganapathy, and B. P. Gupta, Lab Chip **10**(2), 220–226 (2010).
[13]P. Rezai, S. Salam, P. R. Selvaganapathy, and B. P. Gupta, Biomicrofluidics **5**(4), 44116–441169 (2011).
[14]T. U. Biber and M. L. Sanders, J. Gen. Physiol. **61**(5), 529–551 (1973).
[15]C. Martin-Granados, A. R. Prescott, N. Van Dessel, A. Van Eynde, M. Arocena, I. P. Klaska, J. Gornemann, M. Beullens, M. Bollen, J. V. Forrester, and C. D. McCaig, PLoS ONE **7**(7), E40769 (2012).
[16]M. B. A. Djamgoz, M. Mycielska, Z. Madeja, S. P. Fraser, and W. Korohoda, J. Cell. Sci. **114**(14), 2697–2705 (2001).
[17]J. Pu, C. D. McCaig, L. Cao, Z. Zhao, J. E. Segall, and M. Zhao, J. Cell. Sci. **120**(19), 3395–3403 (2007).
[18]C. W. Huang, J. Y. Cheng, M. H. Yen, and T. H. Young, Biosens. Bioelectron. **24**(12), 3510–3516 (2009).
[19]X. Yan, J. Han, Z. Zhang, J. Wang, Q. Cheng, K. Gao, Y. Ni, and Y. Wang, Bioelectromagnetics **30**(1), 29–35 (2009).
[20]L. F. Jaffe, Nature **265**(5595), 600–602 (1977).
[21]M. Poo and K. R. Robinson, Nature **265**(5595), 602–605 (1977).
[22]S. McLaughlin and M. M. Poo, Biophys. J. **34**(1), 85–93 (1981).
[23]M. Zhao, H. Bai, E. Wang, J. V. Forrester, and C. D. McCaig, J. Cell. Sci. **117**(3), 397–405 (2004).
[24]H. Bai, J. V. Forrester, and M. Zhao, Cytokine **55**(1), 110–115 (2011).
[25]V. A. McBain, J. V. Forrester, and C. D. McCaig, Invest. Ophthalmol. Visual Sci. **44**(2), 540–547 (2003).
[26]N. Ozkucur, S. Perike, P. Sharma, and R. H. Funk, BMC Cell Biol. **12**, 4 (2011).
[27]N. Ozkucur, T. K. Monsees, S. Perike, H. Q. Do, and R. H. Funk, PLoS ONE **4**(7), E6131 (2009).
[28]A. M. Rajnicek, L. E. Foubister, and C. D. McCaig, J. Cell. Sci. **119**(9), 1723–1735 (2006).
[29]M. Zhao, B. Song, J. Pu, T. Wada, B. Reid, G. Tai, F. Wang, A. Guo, P. Walczysko, Y. Gu, T. Sasaki, A. Suzuki, J. V. Forrester, H. R. Bourne, P. N. Devreotes, C. D. McCaig, and J. M. Penninger, Nature **442**(7101), 457–460 (2006).
[30]C. W. Huang, H. Y. Chen, M. H. Yen, J. J. Chen, T. H. Young, and J. Y. Cheng, PLoS ONE **6**(10), E25928 (2011).
[31]Y. S. Sun, S. W. Peng, K. H. Lin, and J. Y. Cheng, Biomicrofluidics **6**(1), 14102–1410214 (2012).
[32]C. C. Wang, Y. C. Kao, P. Y. Chi, C. W. Huang, J. Y. Lin, C. F. Chou, J. Y. Cheng, and C. H. Lee, Lab Chip **11**(4), 695–699 (2011).
[33]R. F. Stump and K. R. Robinson, J. Cell Biol. **97**(4), 1226–1233 (1983).
[34]B. Song, Y. Gu, J. Pu, B. Reid, Z. Zhao, and M. Zhao, Nat. Protoc. **2**(6), 1479–1489 (2007).
[35]R. Nuccitelli and C. A. Erickson, Exp. Cell Res. **147**(1), 195–201 (1983).
[36]F. Lin, F. Baldessari, C. C. Gyenge, T. Sato, R. D. Chambers, J. G. Santiago, and E. C. Butcher, J. Immunol. **181**(4), 2465–2471 (2008).
[37]J. Li and F. Lin, Trends Cell Biol. **21**(8), 489–497 (2011).
[38]S. Li, B. P. Chen, N. Azuma, Y. L. Hu, S. Z. Wu, B. E. Sumpio, J. Y. Shyy, and S. Chien, J. Clin. Invest. **103**(8), 1141–1150 (1999).
[39]See supplementary material at http://dx.doi.org/10.1063/1.4749826 for supporting text, figures and tables.
[40]J. Y. Cheng, C. W. Wei, K. H. Hsu, and T. H. Young, Sens. Actuators B **99**(1), 186–196 (2004).
[41]J. Y. Cheng, M. H. Yen, C. T. Kuo, and T. H. Young, Biomicrofluidics **2**(2), 24105 (2008).
[42]Y. W. Chu, P. C. Yang, S. C. Yang, Y. C. Shyu, M. J. Hendrix, R. Wu, and C. W. Wu, Am. J. Respir. Cell Mol. Biol. **17**(3), 353–360 (1997).
[43]J. J. Chen, K. Peck, T. M. Hong, S. C. Yang, Y. P. Sher, J. Y. Shih, R. Wu, J. L. Cheng, S. R. Roffler, C. W. Wu, and P. C. Yang, Cancer Res. **61**(13), 5223–5230 (2001).
[44]N. F. Erdem, E. R. Carlson, D. A. Gerard, and A. T. Ichiki, J. Oral Maxillofac Surg. **65**(9), 1725–1733 (2007).
[45]F. Momose, T. Araida, A. Negishi, H. Ichijo, S. Shioda, and S. Sasaki, J. Oral Pathol. Med. **18**(7), 391–395 (1989).
[46]G. Fuhr and S. Shirley, J. Micromech. Microeng. **5**, 77 (1995).
[47]R. G. Bacabac, T. H. Smit, S. C. Cowin, J. J. Van Loon, F. T. Nieuwstadt, R. Heethaar, and J. Klein-Nulend, J. Biomech. **38**(1), 159–167 (2005).
[48]M. D. Abramoff, P. J. Magalhaes, and S. J. Ram, Biophotonics Int. **11**(7), 36–42 (2004).
[49]D. P. Gaver and S. M. Kute, Biophys. J. **75**(2), 721–733 (1998).
[50]G. Cinamon and R. Alon, J. Immunol. Methods **273**(1-2), 53–62 (2003).
[51]S. Li, N. F. Huang, and S. Hsu, J. Cell. Biochem. **96**(6), 1110–1126 (2005).
[52]H. S. Hele-Shaw, Nature **58**, 34–36 (1898).
[53]P. Gondret, N. Rakotomalala, M. Rabaud, D. Salin, and P. Watzky, Phys. Fluids **9**(6), 1841–1843 (1997).
[54]T. H. Hsu, M. H. Yen, W. Y. Liao, J. Y. Cheng, and C. H. Lee, Lab Chip **9**(7), 884–890 (2009).
[55]M. Zhao, A. Agius-Fernandez, J. V. Forrester, and C. D. McCaig, J. Cell. Sci. **109**(6), 1405–1414 (1996).
[56]J. Pu and M. Zhao, J. Cell. Sci. **118**(6), 1117–1128 (2005).
[57]H. P. Grimm, A. B. Verkhovsky, A. Mogilner, and J. J. Meister, Eur. Biophys. J. **32**(6), 563–577 (2003).
[58]K. Li, E. D. Miller, M. Chen, T. Kanade, L. E. Weiss, and P. G. Campbell, Med. Image Anal. **12**(5), 546–566 (2008).
[59]O. Debeir, I. Adanja, N. Warzee, P. Van Ham, and C. Decaestecker, "Phase contrast image segmentation by weak watershed transform assembly," in *Proceedings of 5th IEEE international symposium on biomedical imaging: From nano to macro (ISBI)*, Paris, France, pp.724–727, 2008
[60]A. J. Hand, T. Sun, D. C. Barber, D. R. Hose, and S. MacNeil, J. Microsc. **234**(1), 62–79 (2009).
[61]M. E. Ambuhl, C. Brepsant, J. J. Meister, A. B. Verkhovsky, and I. F. Sbalzarini, J. Microsc. **245**(2), 161–170 (2012).